

An Inductive Hybrid UPQC for Power Quality Management in Premium-Power-Supply-Required Applications

JIAQI YU¹, (Member, IEEE), YONG XU², YONG LI³, (Senior Member, IEEE),
AND QIANYI LIU³, (Member, IEEE)

¹College of Electronic Information and Electrical Engineering, Changsha University, Changsha 410022, China

²State Grid Hunan Integrated Energy Service Company Ltd., Changsha 410007, China

³College of Electrical and Information Engineering, Hunan University, Changsha 410082, China

Corresponding author: Yong Li (yongli@hnu.edu.cn)

This work was supported in part by the National Natural Science Foundation of China (NSFC) under Grant No. 51822702 and 61572514, and in part by the CERNET Innovation Project under Grant No. NGII20170407.

ABSTRACT Voltage sag and harmonic pollution have a serious impact on the medium-voltage premium-power-supply-required park represented by optical semiconductors, data storage, precision instruments and biopharmaceuticals. Which makes existing equipment require higher voltage capacity of power electronics, higher economic cost and compensation performance. In this paper, an Inductive Hybrid Unified Power Quality Conditioner (IH-UPQC), which is characterized as high integration, reduced DC-link voltage and satisfactory harmonic isolation of transformer, is presented to realize the bi-directional power quality improvement for medium-voltage premium-power-supply-required park. First, the three-phase equivalent circuit and mathematical model are established to reveal the mechanism of harmonic suppression and voltage regulation. Based on the theoretical analysis, the compound control strategy of series and shunt Hybrid Active Power Filter (HAPF) as well as the synchronous method sliding Goertzel discrete Fourier transformation-pre-filtering Phase Lock Loop (PLL) are designed. Then, the main circuit components design including Double Resonant Passive Filter (DRPF), L-C-R low pass filter and the special designed filtering winding for implementing inductive filtering method are described. Finally, the performance of IH-UPQC is validated in 10kV distribution network by MATLAB/Simulink. The simulation results demonstrate that the IH-UPQC is effective to perform grid voltage regulation, load harmonic current suppression and reactive power compensation.

INDEX TERMS Inductive filtering method, unified power quality conditioner (UPQC), double resonant passive filter (DRPF), neutral point converter (NPC), synchronous reference frame (SRF), hybrid active power filter (HAPF), power quality (PQ), phase lock loop (PLL).

I. INTRODUCTION

Currently, the extensive use of Nonlinear Load (NL) and increasing penetration of Renewable Energy Generation (REG) make the medium-voltage premium-power-supply-required park highly vulnerable to Power Quality (PQ) problems. As the key component of NL and REG, power electronic devices are the most responsible ones for abnormal harmonic currents and reactive demand in distribution network,

The associate editor coordinating the review of this manuscript and approving it for publication was Zhigang Liu.

whereas they also require ideal supply voltage for proper operation. The Unified Power Quality Conditioner (UPQC) can not only compensate harmonics and reactive power, but also ensure a regulated load voltage, which makes it the most attractive compensator at distribution network level [1]–[6].

Generally, the traditional UPQC is installed at grid side or NL/REG side, different UPQC wiring schemes in distribution network are shown in Fig.1. In Fig.1 (a), the UPQC is installed at grid side and the NL/REG interfaces with grid via a special transformer. Assuming that the grid voltage and load current are distorted, by analyzing the harmonic flowing path

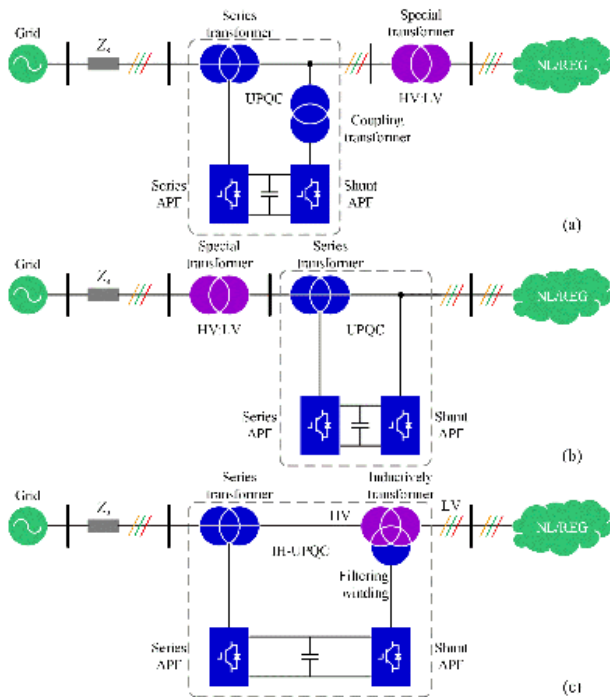


FIGURE 1. Different UPQC wiring schemes in distribution network. (a) Traditional UPQC located at grid side, (b) Traditional UPQC located at NL/REG side, (c) IH-UPQC topology.

in Fig.1 (a), it can be found that the load harmonic current flows into the special transformer and then induces harmonic leakage flux in transformer, which inevitably causes a series of problems to the transformer, such as additional iron and copper losses, noise, vibration and temperature rise, etc. For this typical wiring scheme, the UPQC is effective in isolating harmonics away from public grid and maintaining a regulated load voltage, but it cannot mitigate the negative effects of harmonics on the transformer. In Fig.1 (b), the UPQC is installed at NL/REG side. The special transformer still has to suffer all the distorted voltages, which definitely introduces harmonic leakage flux in the transformer. More importantly, when UPQC is directly parallel with the converter-based REG, it may results in stability problem according to the Extra Element Theorem of Middlebrook [7].

UPQC systems can perform, simultaneously, the series-parallel active power-line compensation by using both series and parallel Active Power Filters (APFs) [8]. The practical implementation of a 3P4W distribution system based on UPQC topology is presented in [9], which can be connected either in 3P3W or in 3P4W distribution power systems, to perform active power-line conditioning by dual compensating strategy implementation, while it only suitable for low voltage system. In [10], a simplified control technique for a dual three-phase topology of a unified power quality conditioner is proposed, which has the series filter controlled as a sinusoidal current source and the shunt filter controlled as a sinusoidal voltage source and can deal with a well-known frequency spectrum, while it cannot inherit traditional UPQC

shown in Fig.1 (a) and Fig.1 (b). Literature [11] proposes a new reduced switch UPQC system topology that comprises of ten switches to reduce the overall switch count of the back-to-back UPQC system while retaining its operational features without any performance tradeoff, while the two shared switches bear much switching loss. To reduce the devices voltage requirements, literature [12] presents a topology that has a reduced DC-link voltage without compromising its compensation capability and helps to match the DC-link voltage requirement of the shunt and series active filters of the UPQC, it also can be applied to higher voltage situation. To enhance the power quality in the medium/high voltage distribution power systems and reduce the devices voltage requirements, a single-phase UPQC based on the M3C is presented in [13], while it increases control complexity for digital implementation. Campanhol *et al.* [14], [15] proposes a single-stage three-phase four-wire grid-connected Photo Voltaic (PV) system operating with a dual compensating strategy and feed forward control loop, the three level Neutral Point Converter (NPC) power circuit gives lower economic cost and better output performance, while this system may results in stability problem between loads and PV system.

Inductive Power Filtering (IPF) method proposed by Li and Luo can mitigate the negative effects of harmonics on the transformer and achieve harmonic suppression near the harmonic sources [16], [17]. The original IPF method adopts a set of single tuned filters to compensate harmonics, but the performance of these passive filters is limited. In fact, harmonic suppression conducted by inductive filtering method has been effectively addressed, but very few of these researches have been undertaken for simultaneous voltage regulation.

Unlike the aforementioned UPQC wiring schemes, this article presents an Inductive Hybrid UPQC (IH-UPQC) shown in Fig.1 (c), which is characterized as high integration, reduced DC-link voltage and satisfactory harmonic isolation of transformer for medium-voltage premium-power-supply-required park. The IH-UPQC integrates the shunt Hybrid Active Power Filter (HAPF) with the Inductive Filtering Transformer (IFT) to implement the inductive filtering method for mitigating the negative effects of harmonics on the transformer. Moreover, the IH-UPQC has a natural advantage of damping resonance due to the isolation characteristic of transformer.

The rest of the article is organized as follows. Section II proposes the IH-UPQC topology. Section III establishes the equivalent circuit and mathematical mode. Section IV gives Sliding Goertzel Discrete Fourier Transformation (SGDFT)-based Phase Lock Loop (PLL), the series APF and shunt HAPF digital control method. Section V. describes the main circuit components design method. The detailed simulation cases in 10kV distribution network are conducted in Section VI. Finally, the conclusion is given in Section VII.

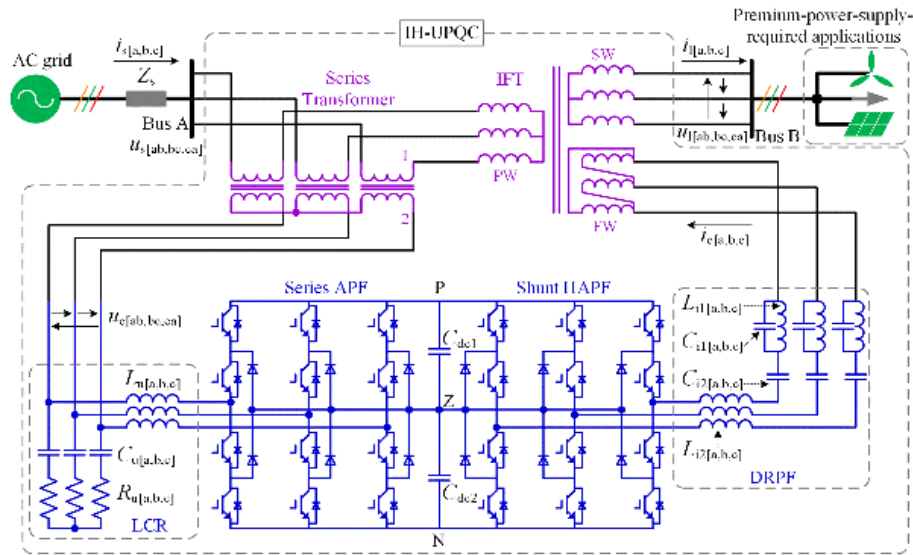


FIGURE 2. Basic system configuration of the IH-UPQC.

II. IH-UPQC TOPOLOGY

The basic system configuration of IH-UPQC is illustrated in Fig. 2. The system is composed of an IFT, a series transformer, an UPQC consisted of a series APF and a shunt HAPF, and the premium-power-supply-required applications, such as wind generation, photovoltaic generation and other sensitive nonlinear load, etc. The shunt HAPF and series APF are based on neutral point converter and connected back-to-back. The passive filter of shunt HAPF is a Double Resonant Passive Filter (DRPF) which has two resonant frequencies and can bear more voltage, while the output filter of series APF is a LCR-Low Pass Filter (LPF). The IFT with YYD wiring has a three-winding structure, its Primary Winding (PW) is connected to public grid via the series transformer, the Secondary Winding (SW) is connected with the premium-power-supply-required applications, and the Filtering Winding (FW) is connected with the shunt HAPF. The IFT and shunt HAPF are used to implement inductive filtering method, where the harmonic magnetic potential balance between SW and FW is reached, which means that the harmonic leakage flux in SW will be offset by the one in FW, thus there are few harmonics in the PW. Furthermore, the series APF is controlled as a non-sinusoidal voltage source to tackle all voltage-related problems for the load, such as voltage harmonics, voltage unbalance, and voltage sag/swell.

Benefited from this integrated configuration, the IH-UPQC inherits the advantages of traditional UPQC, i.e., it suppresses harmonics and compensates reactive power for grid (bus A), and ensure a regulated load voltage for NL/REG (bus B). Moreover, the IH-UPQC gives three main special features: 1) high integration; 2) low DC-link voltage; 3) satisfactory harmonic isolation of transformer.

III. IH-UPQC OPERATING PRINCIPLE

A. EQUIVALENT CIRCUIT MODEL

According to Fig. 2, the NL/REG, especially current-source type NL/REG, can be seen as a non-sinusoidal current source connected in parallel with an impedance. Similar like the current-source type NL/REG, the shunt HAPF is described as a non-sinusoidal current source in parallel with its output impedance. The series APF is equivalent to a controlled voltage source. Thus, the three-phase equivalent circuit model for IH-UPQC is established, as shown in Fig.3. In Fig. 2, $u_{s[ab, bc, ca]}$ represent grid line-to-line voltages, $u_{c[ab, bc, ca]}$ represent line-to-line compensation voltages of series APF, $u_{l[ab, bc, ca]}$ represent line-to-line voltages of the NL/REG. In Fig. 3, $u_{s[a, b, c]}$ represent grid voltages, $u_{c[a, b, c]}$ represent compensation voltages of series APF, $i_{s[a, b, c]}$ represent grid currents, $u_{[a, b, c]n1}$ represent voltages on PW. $i_{l[a, b, c]}$ represent load currents, $u_{[a, b, c]o}$ represent voltages on SW. $u_{[ab, bc, ca]f}$ represent voltages on FW, $i_{[a, b, c]f}$ represent currents on FW, $i_{c[a, b, c]}$ represent compensation currents, $i_{r[a, b, c]}$ represent reference currents of shunt HAPF, $i_{z[a, b, c]}$ represent currents in output impedance Z_o of shunt HAPF. The equivalent impedances of PW, SW and FW are Z_1 , Z_2 , Z_3 , respectively. Besides, as the IH-UPQC is installed between high-voltage power system and low-voltage NL/REG, series transformer and IFT are both step-down transformer, the ratios are $N_1 : N_2$ and $N_{11} : N_{12} : N_{13}$, respectively.

B. HARMONIC CURRENT COMPENSATION MECHANISM

The shunt HAPF operates to compensate harmonics generated by NL/REG and make grid current $i_{s[a, b, c]}$ sinusoidal. The detailed harmonic current compensation mechanism will be revealed in this section. According to transformer

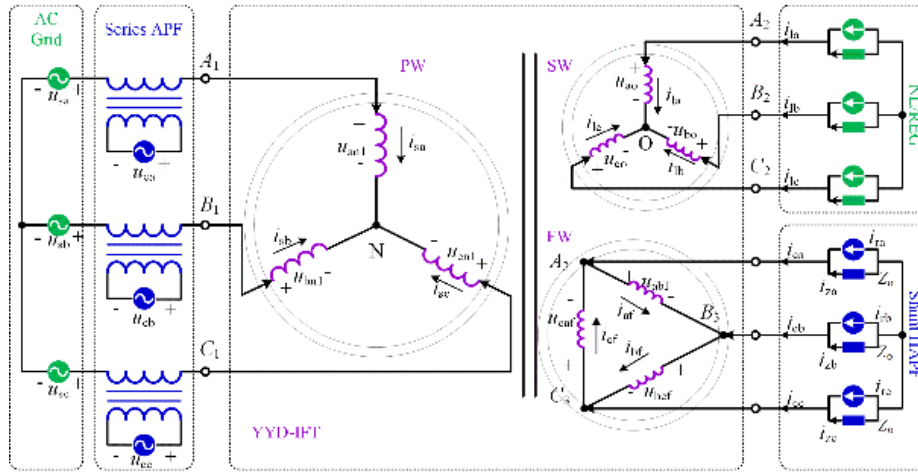


FIGURE 3. The equivalent circuit of basic system.

magnetic potential balance principle, the currents in three windings satisfy the following equations:

$$\begin{cases} N_{11}i_{sa} + N_{12}i_{la} + N_{13}i_{af} = 0 \\ N_{11}i_{sb} + N_{12}i_{lb} + N_{13}i_{bf} = 0 \\ N_{11}i_{sc} + N_{12}i_{lc} + N_{13}i_{cf} = 0 \end{cases} \quad (1)$$

Also, voltage equations of multi-winding transformer can be obtained as follows,

$$\begin{cases} u_{an1} - \frac{N_{11}}{N_{13}}u_{abf} = i_{sa}Z_1 - \frac{N_{11}}{N_{13}}i_{af}Z_3 \\ u_{bn1} - \frac{N_{11}}{N_{13}}u_{bcf} = i_{sb}Z_1 - \frac{N_{11}}{N_{13}}i_{bf}Z_3 \\ u_{cn1} - \frac{N_{11}}{N_{13}}u_{caf} = i_{sc}Z_1 - \frac{N_{11}}{N_{13}}i_{cf}Z_3 \end{cases} \quad (2)$$

According to Kirchhoff's Current Law (KCL), the knot-voltage equations in FW and knot-current equations can be written as:

$$\begin{cases} u_{abf} = i_{zb}Z_{ob} - i_{za}Z_{oa} = (i_{zb} - i_{za})Z_o \\ u_{bcf} = i_{zc}Z_{oc} - i_{zb}Z_{ob} = (i_{zc} - i_{zb})Z_o \\ u_{caf} = i_{za}Z_{oa} - i_{zc}Z_{oc} = (i_{za} - i_{zc})Z_o \end{cases} \quad (3)$$

Similarly, the knot-voltage equations in FW are given by,

$$\begin{cases} i_{sa} + i_{sb} + i_{sc} = 0 \\ i_{la} + i_{lb} + i_{lc} = 0 \\ i_{af} + i_{bf} + i_{cf} = 0 \\ i_{af} = i_{cf} + i_{ca} = i_{cf} + i_{ra} + i_{za} \\ i_{bf} = i_{af} + i_{cb} = i_{af} + i_{rb} + i_{zb} \\ i_{cf} = i_{bf} + i_{cc} = i_{bf} + i_{rc} + i_{zc} \end{cases} \quad (4)$$

According to the mathematical model expressed by (1)-(4), grid currents can be deduced as follows:

$$\begin{cases} i_{sa} = \frac{u_{an1} - \frac{N_{11}}{N_{13}}(i_{ra} - i_{rb})Z_o - \frac{N_{11}N_{12}}{N_{13}^2}(Z_3 + 3Z_o)i_{la}}{Z_1 + \frac{N_{11}^2}{N_{13}^2}(Z_3 + 3Z_o)} \\ i_{sb} = \frac{u_{bn1} - \frac{N_{11}}{N_{13}}(i_{rb} - i_{rc})Z_o - \frac{N_{11}N_{12}}{N_{13}^2}(Z_3 + 3Z_o)i_{lb}}{Z_1 + \frac{N_{11}^2}{N_{13}^2}(Z_3 + 3Z_o)} \\ i_{sc} = \frac{u_{cn1} - \frac{N_{11}}{N_{13}}(i_{rc} - i_{ra})Z_o - \frac{N_{11}N_{12}}{N_{13}^2}(Z_3 + 3Z_o)i_{lc}}{Z_1 + \frac{N_{11}^2}{N_{13}^2}(Z_3 + 3Z_o)} \end{cases} \quad (5)$$

According to equation (5), grid currents are mainly affected by the primary voltages, reference currents of shunt HAPF, and load currents in NL/REG. Assuming that the primary harmonic voltages are compensated completely, i.e., for harmonic currents, $u_{uah} = u_{ubh} = u_{uch} = 0$. in order to ensure that no load harmonic currents induct into primary winding, i.e., for harmonic currents, $i_{sa} = i_{sb} = i_{sc} = 0$, the shunt HAPF reference currents (i_{ra} , i_{rb} , i_{rc}) should meet the following expressions [18]:

$$\begin{cases} i_{ra} = \frac{N_{12}}{N_{13}} \frac{(Z_3 + 3Z_o)}{3Z_o} (i_{lc} - i_{la}) \\ i_{rb} = \frac{N_{12}}{N_{13}} \frac{(Z_3 + 3Z_o)}{3Z_o} (i_{la} - i_{lb}) \\ i_{rc} = \frac{N_{12}}{N_{13}} \frac{(Z_3 + 3Z_o)}{3Z_o} (i_{lb} - i_{lc}) \end{cases} \quad (6)$$

Actually, in order to eliminate the adverse effect of Z_3 on filtering performance and stability, Z_3 is designed close

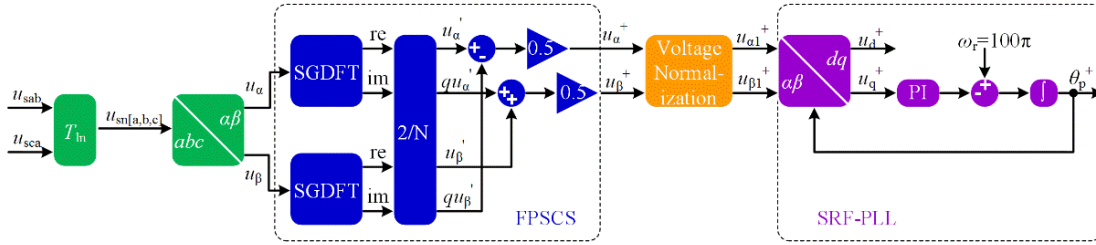


FIGURE 4. Block diagram of SGDFT-pre-filtering PLL.

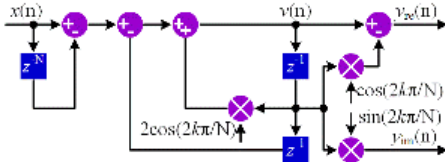


FIGURE 5. Realization diagram of SGDFT.

to zero-impedance, which is the precondition for the implementation of inductive filtering method. Therefore, reference currents can be simplified as (7).

$$\begin{cases} i_{ra} = \frac{N_{i2}}{N_{i3}}(i_{lc} - i_{la}) \\ i_{rb} = \frac{N_{i2}}{N_{i3}}(i_{la} - i_{lb}) \\ i_{rc} = \frac{N_{i2}}{N_{i3}}(i_{lb} - i_{lc}) \end{cases} \quad (7)$$

C. VOLTAGE COMPENSATION MECHANISM

The series APF operates to maintain NL/REG voltages balanced and sinusoidal with the desired amplitude. The proposed series APF regulates NL/REG voltages by

controlling secondary open circuit voltages of IFT. In no-load condition, secondary open circuit voltages can be described as,

$$\begin{cases} u_{ao} = \frac{N_{i1}}{N_{i2}}u_{an1} \\ u_{bo} = \frac{N_{i1}}{N_{i2}}u_{bn1} \\ u_{co} = \frac{N_{i1}}{N_{i2}}u_{cn1} \end{cases} \quad (8)$$

According to the principle of electromagnetic induction and Kirchhoff's Voltage Law (KVL), the primary voltages can be expressed as,

$$\begin{cases} u_{an1} = u_{sa} + \frac{N_1}{N_2}u_{ca} \\ u_{bn1} = u_{sb} + \frac{N_1}{N_2}u_{cb} \\ u_{cn1} = u_{sc} + \frac{N_1}{N_2}u_{cc} \end{cases} \quad (9)$$

Equations (8) and (9) indicate that once primary voltages deviates from the rated value, series APF will inject series

voltages $u_{c[a,b,c]}$ to promise a regulated load voltage. Combining equations (8) and (9), the reference voltages $u_{cr[a,b,c]}$ are given by,

$$\begin{cases} u_{cra} = \left(\frac{N_{i1}}{N_{i2}}u_{La}^* - u_{sa} \right) \frac{N_2}{N_1} \\ u_{crb} = \left(\frac{N_{i1}}{N_{i2}}u_{Lb}^* - u_{sb} \right) \frac{N_2}{N_1} \\ u_{crc} = \left(\frac{N_{i1}}{N_{i2}}u_{Lc}^* - u_{sc} \right) \frac{N_2}{N_1} \end{cases} \quad (10)$$

where $u_{L[a,b,c]}^*$ are the nominal-NL/REG voltages.

IV. SRF-BASED COMPOUND CONTROL

The proposed IH-UPQC compound control structure is based on Synchronous Reference Frame (SRF), where the shunt HAPF and series APF are regulated in an independent way. The shunt HAPF compensates harmonic current and regulates DC-link voltage by dual-loop feedback and voltage feed-forward scheme. The series APF utilizes voltage feedback and current feedforward scheme to regulate deviated load voltage.

A. SGDFT-PRE-FILTERING PLL

As both series and shunt HAPF need to keep synchronization with grid, while the traditional SRF-PLL gives poor performance under non-ideal grid voltage, this article introduces a pre-filtering SRF-PLL based on SGDFT. The block diagram of SGDFT-pre-filtering PLL is illustrated in Fig. 4. Its structure is composed of three parts: Fundamental Positive Sequence Components Separation (FPSCS), voltage normalization and SRF-PLL. The FPSCS module uses SGDFT filter [20] and symmetrical component method [19] to separate FPSC even under abnormal grid voltage. SRF-PLL is adopted in order to calculate grid fundamental positive sequence phase. Voltage normalization is employed to remove the adverse effect of variable input voltage amplitude on SRF-PLL.

In Fig. 4, T_{in} is used to achieve equivalent transform from line-to-line voltages to phase voltages, and its expression is,

$$\begin{bmatrix} u_{sna} \\ u_{snb} \\ u_{snc} \end{bmatrix} = \frac{1}{3} \begin{bmatrix} 1 & -1 & \\ -2 & -1 & \\ 1 & 2 & \end{bmatrix} \begin{bmatrix} u_{sab} \\ u_{sca} \end{bmatrix} \quad (11)$$

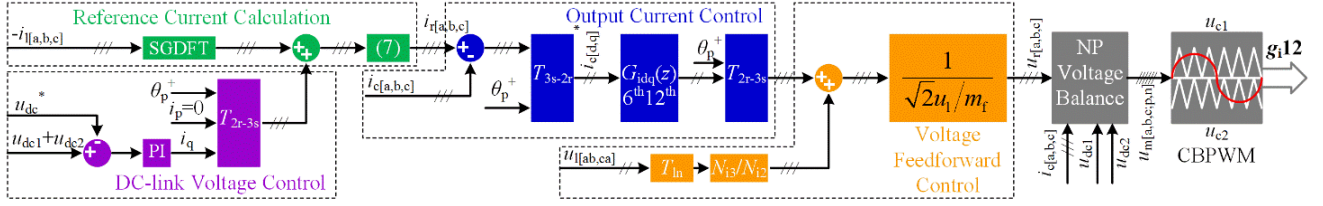


FIGURE 6. Control diagram of shunt HAPF.

The transformation expressions of $abc-\alpha\beta$, $\alpha\beta-dq$ and voltage normalization are as follows,

$$\begin{aligned} T_{abc-\alpha\beta} &= \frac{2}{3} \begin{bmatrix} 1 & -1/2 & -1/2 \\ 0 & \sqrt{3}/2 & -\sqrt{3}/2 \end{bmatrix} \\ T_{\alpha\beta-dq} &= \begin{bmatrix} \cos \theta_p^+ & \sin \theta_p^+ \\ -\sin \theta_p^+ & \cos \theta_p^+ \end{bmatrix}, \\ \begin{bmatrix} u_{\alpha 1}^+ \\ u_{\beta 1}^+ \end{bmatrix} &= \begin{bmatrix} u_{\alpha}^+ / \sqrt{u_{\alpha}^2 + u_{\beta}^2} \\ u_{\beta}^+ / \sqrt{u_{\alpha}^2 + u_{\beta}^2} \end{bmatrix} \end{aligned} \quad (12)$$

SGDFT filter has satisfactory filtering ability at the frequencies that are integer times of fundamental frequency. Its transfer function and realization diagram are shown below,

$$G_{SGDFT}(z) = \frac{(1 - e^{-j2k\pi/N} z^{-1})(1 - z^{-N})}{1 - 2 \cos(2k\pi/N) z^{-1} + z^{-2}} \quad (13)$$

where k is frequency domain index and N is the sampling number.

According to the symmetrical component method, fundamental positive sequence components $u_{\alpha}^+ u_{\beta}^+$ are obtained by,

$$\begin{bmatrix} u_{\alpha}^+ \\ u_{\beta}^+ \end{bmatrix} = \frac{1}{2} \begin{bmatrix} 1 & j \\ -j & 1 \end{bmatrix} \begin{bmatrix} u'_{\alpha} \\ u'_{\beta} \end{bmatrix} = \frac{1}{2} \begin{bmatrix} u'_{\alpha} - qu'_{\beta} \\ qu'_{\alpha} + u'_{\beta} \end{bmatrix} \quad (14)$$

By the SGDFT-pre-filter, this PLL can operate satisfactorily under seriously abnormal grid voltage as long as the Proportional Integral (PI) gains are properly tuned.

B. COMPOUND CONTROL SCHEME FOR SHUNT HAPF

Fig. 6 shows the control block diagram of the shunt HAPF. It consists of six blocks: reference current calculation, DC-link voltage control, output current control, voltage feed forward control, Neutral Point (NP) voltage balance and Carrier-Based Pulse Width Modulation (CBPWM).

The reference current is extracted from the load current by SGDFT and then calculated according to (7). The DC-link voltage is maintained at a constant reference value u_{dc}^* by a PI controller and the regulated current is overlaid on the reactive axis. Aiming at tracking the current reference, the Proportional Resonant (PR) controller is designed, its transfer function in discrete domain can be deduced by impulse invariant

method [21],

$$\begin{aligned} G_{idq}(s) &= k_{pi} + \sum_{n=6,12} \frac{2k_{in}s}{s^2 + \omega_n^2} \xrightarrow{\text{impulse invariant}} G_{idq}(z) = Z^{-1}\{G_{idq}(s)\} \\ G_{idq}(z) &= k_{pi} + \sum_{n=6,12} \frac{2k_{in}T_s(1 - z^{-1} \cos(\omega_n T_s))}{1 - 2z^{-1} \cos(\omega_n T_s) + z^{-2}} \end{aligned} \quad (15)$$

where k_{pi} is proportional coefficient, k_{in} is integral coefficient, T_s is sampling period, m_f is duty cycle.

Considering that the dominated harmonic orders in load current are 5th, 7th, 11th and 13th, the 6th and 12th PR controllers in dq are adopted. Moreover, voltage feed forward control is employed to eliminate grid voltage disturbances. The NP voltage balance strategy is realized by modulating signals reconstruction. The modulation signals are determined by the variation direction of reference voltage $u_{r[a,b,c]}$, splitting DC-link voltage deviation and output current [22], [23], that is,

$$\begin{cases} u_{map} = u_{ap} + u_{aoff} & u_{mbp} = u_{bp} + u_{boff} & u_{mcp} = u_{cp} + u_{coff} \\ u_{man} = u_{an} - u_{aoff} & u_{mbn} = u_{bn} - u_{boff} & u_{mcn} = u_{cn} - u_{coff} \end{cases} \quad (16)$$

where $u_{m[a,b,c]p}$ and $u_{m[a,b,c]n}$ are reconstructed reference voltages and can be obtained as follows,

$$\begin{cases} u_{ap} + u_{an} = u_{ra} - \frac{\min(u_{ra}, u_{rb}, u_{rc}) + \max(u_{ra}, u_{rb}, u_{rc})}{2} \\ u_{bp} + u_{bn} = u_{rb} - \frac{\min(u_{ra}, u_{rb}, u_{rc}) + \max(u_{ra}, u_{rb}, u_{rc})}{2} \\ u_{cp} + u_{cn} = u_{rc} - \frac{\min(u_{ra}, u_{rb}, u_{rc}) + \max(u_{ra}, u_{rb}, u_{rc})}{2} \end{cases} \quad (17)$$

$u_{c[a,b,c]off}$ are the voltage deviations expressed by,

$$\begin{cases} u_{aoff} = k_t |u_{dc1} - u_{dc2}| \text{sign}((u_{ap} - u_{an} - 1)(u_{dc1} - u_{dc2}) i_{ca}) \\ u_{boff} = k_t |u_{dc1} - u_{dc2}| \text{sign}((u_{bp} - u_{bn} - 1)(u_{dc1} - u_{dc2}) i_{cb}) \\ u_{coff} = k_t |u_{dc1} - u_{dc2}| \text{sign}((u_{cp} - u_{cn} - 1)(u_{dc1} - u_{dc2}) i_{cc}) \end{cases} \quad (18)$$

where k_t is regulation factor.

It determines voltage unbalance regulation degree. The final driving signals are obtained by logical judgment of modulation signals $u_{m[a,b,c;p,n]}$ in CBPWM. The detailed realization diagram of CBPWM method is shown in Fig. 7.

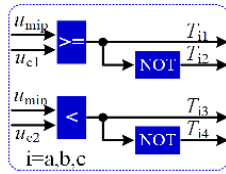


FIGURE 7. Detail diagram of CBPWM.

Combining the above strategy with CBPWM, NP voltage can be well balanced.

C. COMPOUND CONTROL SCHEME FOR SERIES HAPF

Fig. 8 shows the detailed control block diagram for series APF. The control scheme of series APF contains four blocks: reference voltage calculation, output voltage control, current feedforward control and CBPWM.

According to (10), the reference voltages $u_{cr[a,b,c]}$ are deduced by grid voltages $u_{s[ab,ca]}$ and desired load voltages $u_{L[a,b,c]}^*$, which are calculated by fundamental positive sequence phase θ_p^+ and nominal load phase voltage amplitude u_{ln}^* . Similar like the current control of shunt HAPF, 6th and 12th PR controllers expressed as $G_{udq}(z)$ are employed to track the reference voltages. The current feedforward control is also adopted to eliminate the NL/REG current disturbances. Different from shunt HAPF, series APF is not responsible for regulating DC-link and NP voltage. Therefore, there is no need to modify its reference voltage, i.e., u_{ma} of series APF acts the same role as u_{map} and u_{man} of shunt HAPF, so as to u_{mb} and u_{mc} .

V. MAIN CIRCUIT COMPONENTS DESIGN

In principle, harmonic suppression of NL/REG is performed mainly by passive filter of shunt HAPF coordinated with zero impedance designed FW, the active part is responsible for filtering performance improvement. While the voltage regulation is accomplished by active part of series APF, the passive filter only acts as an output filter. These passive components design are discussed in the following subsections.

A. ZERO IMPEDANCE DESIGN OF FILTERING WINDING

According to the analysis in Section III-B, zero impedance design of FW is the precondition to implement inductive filtering method. Thus, practical design method must be introduced [18]. It is known that the equivalent impedance of transformer can be calculated by the short-circuit impedance, that is,

$$Z_3 = \frac{1}{2}(Z_{13} + Z_{23} - Z_{12}) \quad (19)$$

where Z_{12} , Z_{13} , Z_{23} are short circuit impedance between PW and SW, PW and FW, SW and FW, respectively.

The percentage of short-circuit impedance is proportional to the geometry size of windings and the isolation distance between the two corresponding windings. The geometry size of windings are fixed within a certain scale in trans-

former design. Thus, the desired equivalent impedance can be achieved by adjusting isolation distance. According to the special transformer design theory [24], equivalent impedance Z_3 can be simplified as $Z_3 = k_x(d_{13} + d_{23} - d_{12})$, where d_{13} , d_{23} and d_{12} are the isolation distances between PW and FW, SW and FW, PW and FW, respectively. Obviously, if isolation distance satisfies this condition $d_{13} + d_{23} = d_{12}$, zero impedance can be achieved [18]. Fig. 9 shows the winding arrangement of the IFT.

B. DRPF DESIGN FOR SHUNT HAPF

The DRPF which can be equal to two shunt single resonant circuit is adopted in shunt HAPF. DRPF gives three functions for shunt HAPF: 1) low-impedance circuit for two specific harmonics; 2) fixed reactive power compensation; 3) high fundamental voltage dividing ability. Taking phase A as an example, its impedance transfer function is,

$$\begin{aligned} Z(s) &= \frac{L_{i1a}s/C_{i1a}s}{1/C_{i1a}s + L_{i1a}s} + \frac{1}{C_{i2a}s} + L_{i2a}s \\ &= \frac{L_{i1a}L_{i2a}C_{i1a}C_{i2a}s^4 + (L_{i1a}C_{i1a} + L_{i2a}C_{i2a} + L_{i1a}C_{i2a})s^2 + 1}{L_{i1a}C_{i1a}C_{i2a}s^3 + C_{i2a}s} \end{aligned} \quad (20)$$

Fig. 10 shows bode plot of $Z(s)$, it can be observed that $Z(s)$ has two minimum and one maximum at the series resonant frequencies f_1 , f_2 and shunt resonant frequency f_r , respectively. In order to obtain satisfactory filtering characteristics at f_1 and f_2 , f_r is recommended to be set as $(f_1 + f_2)/2$.

When the DRPF occurs series resonance, it can be obtained that,

$$\begin{aligned} Z(\omega) &= -j \frac{L_{i1a}L_{i2a}C_{i1a}C_{i2a}\omega^4}{C_{i2a}\omega - L_{i1a}C_{i1a}C_{i2a}\omega^3} \\ &+ \frac{1 - (L_{i1a}C_{i1a} + L_{i2a}C_{i2a} + L_{i1a}C_{i2a})\omega^2}{C_{i2a}\omega - L_{i1a}C_{i1a}C_{i2a}\omega^3} = 0 \end{aligned} \quad (21)$$

The resonant angular frequency ω_1 , ω_2 can further be expressed as follows:

$$\begin{cases} \omega_1^2 + \omega_2^2 = \frac{L_{i1a}C_{i1a} + L_{i2a}C_{i2a} + L_{i1a}C_{i2a}}{L_{i1a}L_{i2a}C_{i1a}C_{i2a}} \\ \omega_1^2\omega_2^2 = \frac{1}{L_{i1a}L_{i2a}C_{i1a}C_{i2a}} \end{cases} \quad (22)$$

When the DRPF occurs parallel resonance, the reference resonant angular frequency ω_r can be deduced as,

$$\omega_r^2 = L_{i1a}C_{i1a} \quad (23)$$

If the demanded reactive power is Q_c , the fundamental impedance is, where ω_f is the fundamental angular frequency and U_{ph} is input phase voltage RMS of the DRPF. Combining (22), (23) with (24), as shown at the bottom of the next page, it can be figured out that,

$$\frac{U_{ph}^2}{Q_c} = \frac{\omega_f^4\omega_1^2\omega_2^2 - \omega_f^2(\omega_1^2 + \omega_2^2)/(\omega_1^2\omega_2^2) + 1}{C_{i2a}\omega_f(1 - \omega_f^2\omega_r^2)} \Rightarrow$$

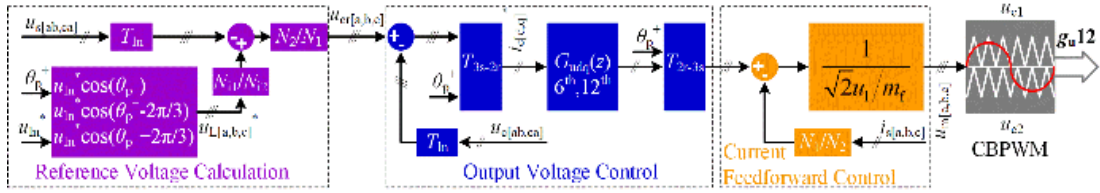


FIGURE 8. Control diagram of series APF.

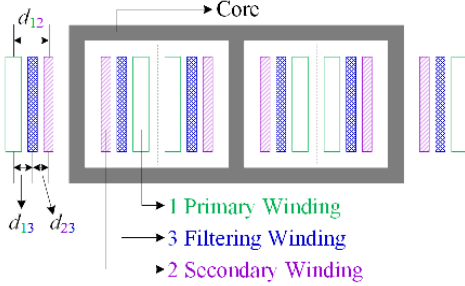
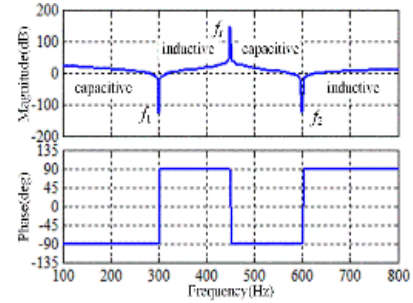


FIGURE 9. Winding arrangement in sectional view.

FIGURE 10. Bode plot of $Z(s)$.

$$C_{i2a} = \frac{Q_c \left[\omega_f^4 \omega_1^2 \omega_2^2 - \omega_f^2 (\omega_1^2 + \omega_2^2) / (\omega_1^2 \omega_2^2) + 1 \right]}{U_{ph}^2 \omega_f (1 - \omega_f^2 \omega_r^2)} \quad (25)$$

Consequently, design rule of L_{i2a} , L_{i1a} and C_{i1a} can be obtained from (22), (23) and (25),

$$\begin{cases} L_{i2a} = \frac{\omega_r^2}{\omega_1^2 \omega_2^2 C_{i2a}} \\ L_{i1a} = \frac{\omega_1^2 \omega_2^2 (\omega_1^2 + \omega_2^2 - \omega_r^2) L_{i2a}}{\omega_1^2 \omega_2^2 \omega_r^2 - 1} \\ C_{i1a} = \frac{1}{\omega_r^2 L_{i1a}} \end{cases} \quad (26)$$

C. LCR-LPF DESIGN FOR SERIES APF

LCR-LPF is utilized to reduce the high order harmonics in the injected voltages of series APF. The voltage transfer function between inverter voltage and compensation voltage is,

$$G_v(s) = \frac{R_u C_u s + 1}{L_u C_u s^2 + R_u C_u s + 1} \quad (27)$$

And the resonance frequency is,

$$f_r = \frac{1}{2\pi \sqrt{L_u C_u}} \quad (28)$$

The design of inductor L_u is the same as the conventional LCL filters, and its value is depend on the bandwidth and filtering performance at low frequency.

When the required compensation harmonic frequency f_{rch} is assigned, f_r should meet the constraint that: $f_{rch} < f_r < f_s/2$. And then, L_u and C_u can be figured out by the above expressions. Moreover, R_u affects the system stability and harmonic tracking ability, a tradeoff between these two aspects should be made in the choice of R_u .

VI. SIMULATION STUDY

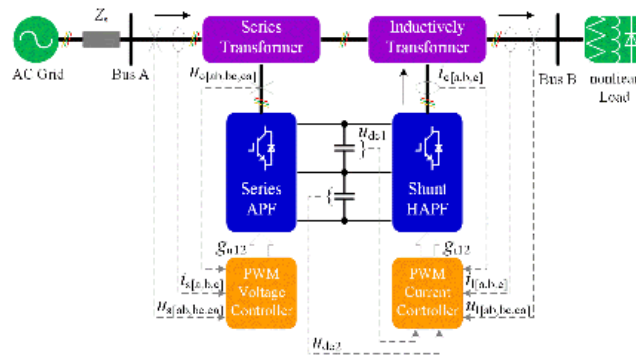
The performance of the proposed IH-UPQC is evaluated in 10kV/0.4kV distribution network by MATLAB/Simulink. The simulation topology is shown in Fig. 11.

The IH-UPQC system is connected between bus A and bus B and in front of a set of nonlinear loads. A thyristor control type converter with RL load is used to simulate the nonlinear load and the angle of trigger is 20° . The system parameters, IFT parameters and control parameters are listed in Table 1. The system parameter is based on the real distribution networks and calculated by Eq.(20)- Eq.(28). IFT parameters are chosen by transformer design method and control parameters are chosen by control performance and system stability. The following typical cases are investigated in detail.

$$\begin{aligned} Z(\omega_f) &= -j \frac{U_{ph}^2}{Q_c} \\ &= -j \frac{L_{i1a} L_{i2a} C_{i1a} C_{i2a} \omega_f^4 - (L_{i1a} C_{i1a} + L_{i2a} C_{i2a} + L_{i1a} C_{i2a}) \omega_f^2 + 1}{-L_{i1a} C_{i1a} C_{i2a} \omega_f^3 + C_{i2a} \omega_f} \end{aligned} \quad (24)$$

TABLE 1. Simulation parameters.

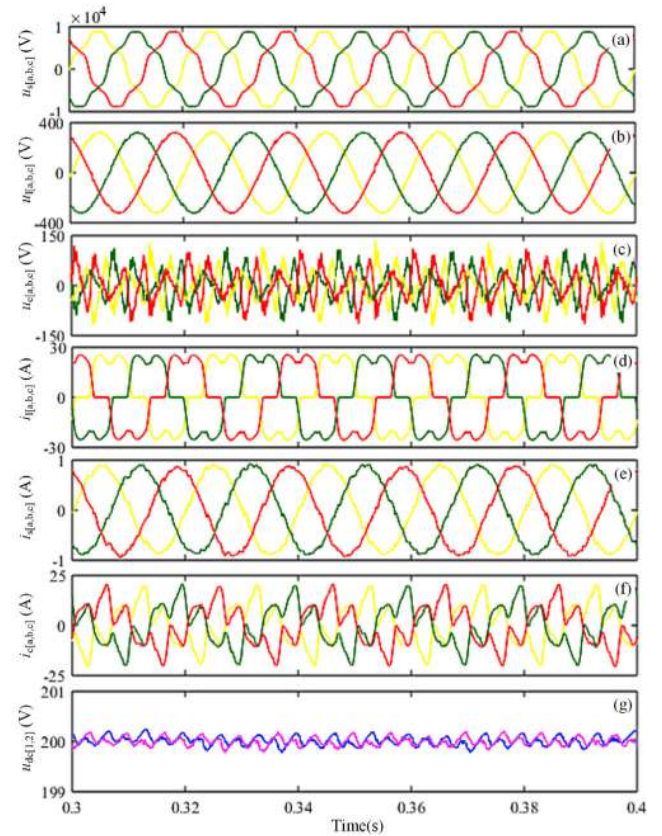
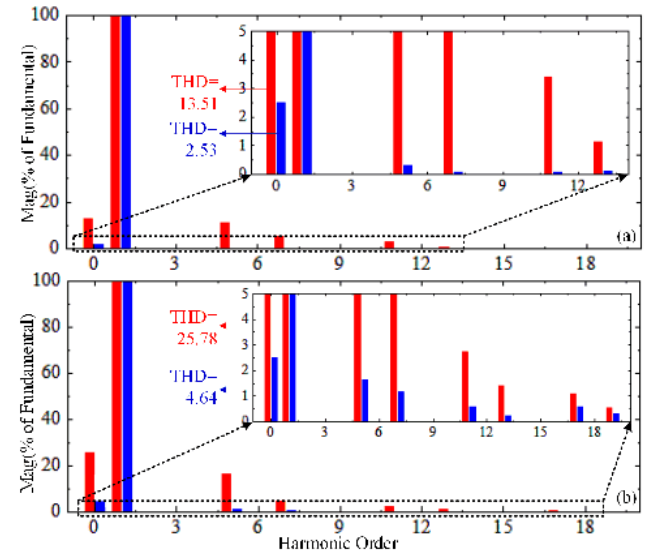
System parameters			
Line-to-line voltage $u_{s[ab,bc,ca]}$		10 kV	
Line frequency f_0		50 Hz	
Grid inductance L_s		0.5 mH	
Grid resistance R_s		0.2 Ω	
Series transformer ratio		5.77kV/0.23kV	
$C_{dc1}=C_{dc}$	9400 μ F	L_u	2 mH
C_u	20 μ F	R_u	6 Ω
L_{i1}	0.58 mH	C_{i1}	215.1 μ F
L_{i2}	1.35 mH	C_{i2}	117.6 μ F
u_{dc}	800 V		
IFT parameters			
Wiring mode	YYD	Rating	630 kVA
Winding voltage u_{an1}	5.77 kV	Equivalent Z_1	0.05 + 0.05j
Winding voltage u_{ao}	0.23kV	Equivalent Z_2	0.25 + 0.25j
Winding voltage u_{abr}	0.4kV	Equivalent Z_3	0.035 + 0.15j
Control parameters			
f_s	12.8 kHz	k_t	0.3
k_{pc}	10	k_{ic6}	640
k_{ic12}	320	k_{pv}	10
k_{iv6}	640	k_{iv12}	320
k_{pdc}	3	k_{ide}	200

**FIGURE 11.** Simulation topology.

A. SIMULTANEOUS GRID VOLTAGE AND LOAD CURRENT HARMONICS COMPENSATION

The performance of IH-UPQC under the condition of grid voltages distortion and nonlinear loads is illustrated in Fig 12. In this condition, distorted grid voltages with characteristic harmonics of 5th, 7th, 11th and 13th are deliberately introduced. The diode rectifier with RL load is also considered in the system. The distorted grid voltage and load current waveforms are given in Fig. 12(a) and (d), respectively. As viewed from Fig. 12(b) and (e), with the IH-UPQC in operation, source currents and load voltages become smooth and sinusoidal. In Fig.12 (g), it is also noticed that both of the splitting NP voltages are regulated at reference value 200 V, which verifies the effectiveness of NP voltage balance method.

For better visualization of compensation performance, Fast Fourier Transform (FFT) analysis of the load voltage and grid current are shown in Fig. 13. Fig. 13 demonstrates that 5th, 7th, 11th and 13th harmonics are eliminated close to zero, and Total Harmonic Distortion (THD) of load voltage and grid current are decreased from 13.51% to 2.53% and 25.78% and 4.64%, respectively.

**FIGURE 12.** Harmonic compensation for grid voltage and load current. (a) Grid phase voltages (b) Load phase voltages (c) Output compensation voltages (d) Load currents, (e) Grid currents (f) Output compensation currents (g) Splitting DC-link voltages.**FIGURE 13.** FFT analysis of phase A grid voltage and load current before and after compensation. (a) Grid phase voltages (b) Load currents.

B. ASYMMETRIC VOLTAGE SAG AND SWELL COMPENSATION

The performance of IH-UPQC under asymmetric voltage sag and swell are given in Fig 14 and Fig 15, respectively.

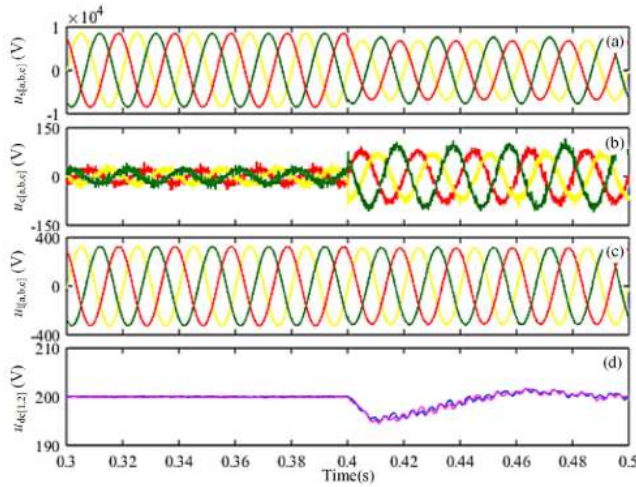


FIGURE 14. Voltage sag compensation. (a) Grid phase voltages (b) Output compensation voltages (c) Load voltages (d) Splitting DC-link voltages.

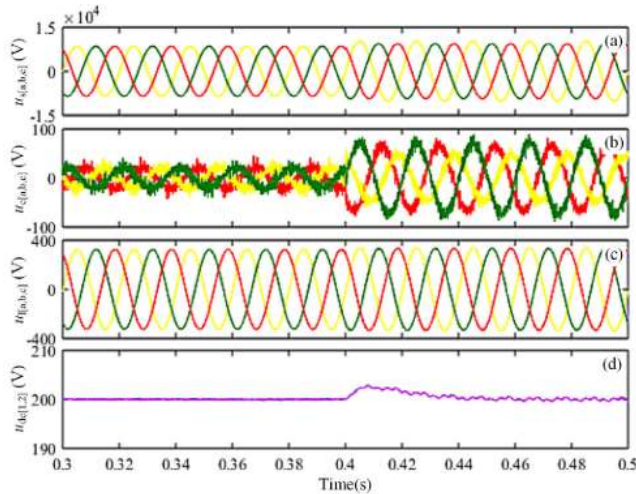


FIGURE 15. Voltage swell compensation. (a) Grid phase voltages (b) Output compensation voltages (c) Load voltages (d) Splitting DC-link voltages.

For voltage sag condition, unbalanced grid voltages with a 20% sag on phase A and C and a 10% sag on phase B are introduced at 0.4s. Similarly, for voltage swell condition, unbalanced grid voltages with a 20% swell on phase A and a 10% swell on phase B and C are introduced at 0.4s. A pure resistive load is considered in the two conditions. As shown in Fig. 14(b) and Fig. 15(b), the IH-UPQC acts immediately to inject appropriate compensating voltages after voltage sag/swell occurs. Consequently, the load voltages are regulated balanced and at the rated value, which can be noticed from Fig. 14(c) and Fig. 15(c). In Fig. 14(d) and Fig. 15(d), both of the splitting NP voltages are maintained at reference value of 400 V within 3% overshoot in two cycles. It is evident that the IH-UPQC is able to maintain the load voltage at its rated value under 20% sag and swell condition.

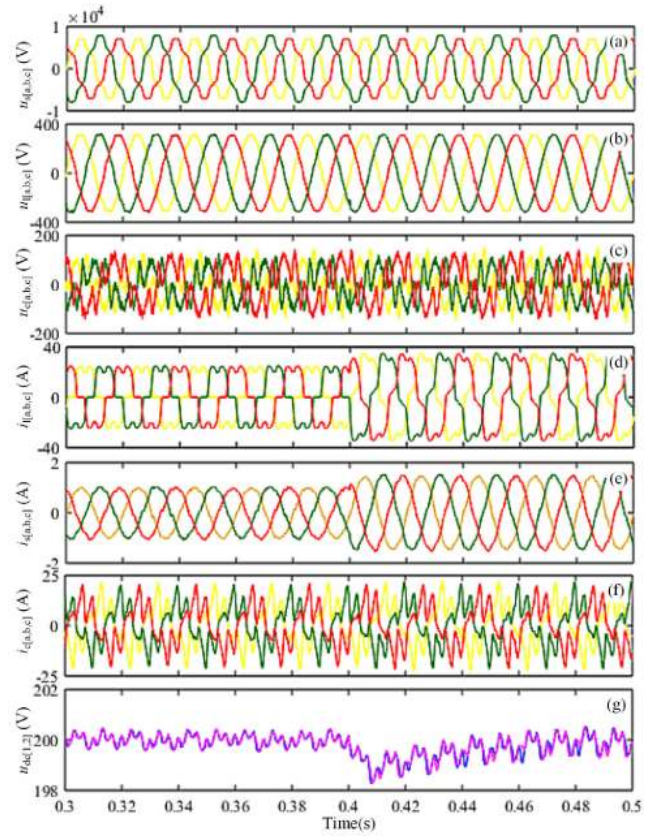


FIGURE 16. Dynamic performance of the IH-UPQC under sudden load change. (a) Grid phase voltages (b) Load phase voltages (c) Output compensation voltages (d) Load currents (e) Grid currents (f) Output compensation currents (g) Splitting DC-link voltages.

C. DYNAMIC RESPONSE OF SUDDEN LOAD CHANGE

This dynamic response is examined in harmonic, unbalance and sag grid voltage with nonlinear load followed by RL load, as it is a more challenging scenario.

As shown in Fig. 16(a), the IH-UPQC puts into operation at 0.3s. Before 0.4s, the series APF regulates the load voltages at the rated value and free of distortion in Fig. 16(b), while the shunt HAPF outputs reference current to isolate harmonic currents from flowing into grid shown in Fig. 16(e). At 0.4s, an extra resistive load is suddenly connected in parallel with the nonlinear load, which gives birth to a load current amplitudes increase shown in Fig. 16(d). From Fig. 16(c) and (f), it can be observed that the output voltages and currents of IH-UPQC do not change with load active power increasing. The changing process of grid current and DC-link voltage are satisfactory: within 3% overshoot and 2 cycles' response time, which can be observed from Fig. 16(e) and (g). The sudden load change does not impose any considerable effect on DC-link voltage. It is evident that the changeover from one operating condition to another is smooth, the IH-UPQC maintain excellent compensation performance irrespective of load change.

To clearly recognize the power variation under load change, the active and reactive power relationships are shown

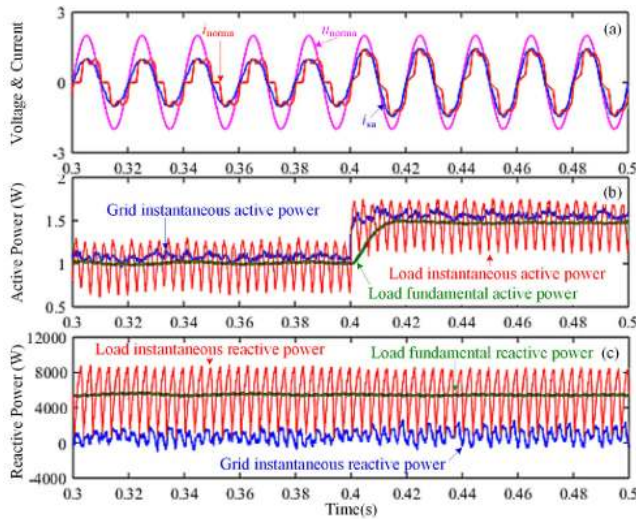


FIGURE 17. Power waveform of grid and load. (a) Normalized phase A voltage, grid current, load current (b) Active power (c) Reactive power.

in Fig. 17. As shown in Fig. 17(a) and (c), before load change, the grid voltage and current are in phase, the grid instantaneous reactive power are stabilized around zero, which means that the load reactive power demand is supplied by the shunt HAPF. In Fig.17, load instantaneous active and reactive power are fluctuant due to the distorted load currents. After load change, the load fundamental active power is still approximately equal to grid instantaneous active power, and grid instantaneous reactive power is approximately equal to zero, which once again strengthens that IH-UPQC do not influence active power flow and it mainly output reactive and harmonic currents.

The simulation indicators are summarized in Table 2. Compensation Rate indicates load voltage deviate from nominal voltage after compensation.

TABLE 2. Simulation indices.

Steady state indices		
	Load voltage	Grid current
THD	2.53%	4.64%
Compensation Rate	$\pm 2\%$	--
Dynamic indices		
Overshoot	1%	5%
Regulation time	10ms	10ms

D. COMPARISON RESULTS BETWEEN IH-UPQC AND THE CONVENTIONAL UPQC

To elaborate the suitability and ability of replacing conventional UPQC with this approach, this subsection gives out the comparison results between IH-UPQC and the conventional UPQC.

As shown in Fig. 18, subscript 1 and 2 represents IH-UPQC and the conventional UPQC, respectively. Grid voltage and load condition are same as the aforementioned conditions. It can be figured out that IH-UPQC can obtain similar steady

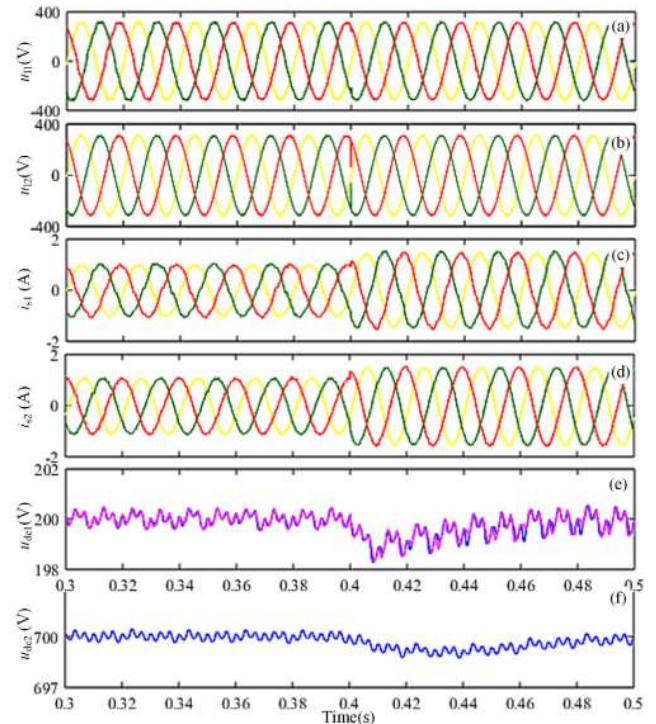


FIGURE 18. Comparison results under sudden load change. (a) Load phase voltages of IH-UPQC (b) Load phase voltages of conventional UPQC (c) Grid currents of IH-UPQC (d) Grid currents of conventional UPQC (e) DC link voltages of H-UPQC (f) DC link voltage of conventional UPQC.

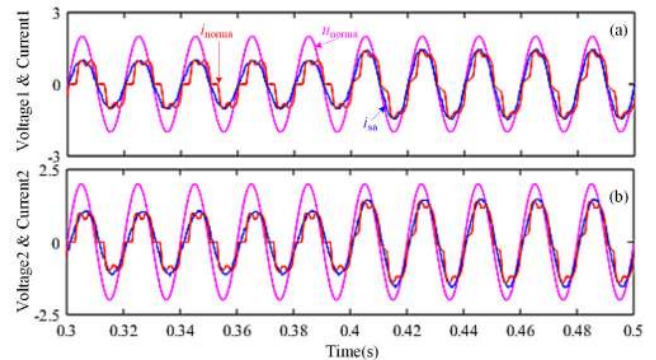


FIGURE 19. Comparison results of reactive power compensation (a) Normalized phase A voltage, grid current, load current of IH-UPQC (b) Normalized phase A voltage, grid current, load current of conventional UPQC.

compensation performance with conventional UPQC. While the conventional UPQC obtains higher overshoot and regulating time than IH-UPQC in voltage compensation and DC voltage regulation. Moreover, IH-UPQC just require half DC-link voltage of conventional UPQC. In Fig. 19, IH-UPQC has another advantage that it can compensate reactive power without increasing inverters capacity.

The cost of IH-UPQC mainly contains IFT, series transformer, back-to-back inverter, passive hybrid filter. In distribution networks, the cost of distribution transformer gives a little lower price than IFT, while the higher capacity back-to-back inverter are more

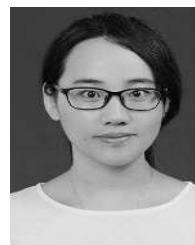
expensive than hybrid back-to-back inverter. Thus, IH-UPQC has suitability and ability for replacing traditional UPQC in medium-voltage scenario.

VII. CONCLUSION

This article proposes an IH-UPQC to improve grid PQ and provide premium power supply for sensitive NL and REG in medium-voltage park. Different from the conventional UPQC, the IH-UPQC integrates shunt HAPF with IFT to implement inductive filtering, which is rewarding to reduce adverse effects of harmonics on the transformer and beneficial to system stability. The three-phase equivalent circuit and mathematical model are established to clarify the mechanism of harmonic suppression and voltage regulation, the realization aspects of control strategy and main circuit components design are discussed. The simulation results indicate that the IH-UPQC not only suppresses harmonics and compensates reactive power near the harmonic source, but also compensates grid voltage harmonics, unbalance and sag simultaneously, which makes the overall distribution power system more clean and healthy. The proposed method has a wide application potentials in industrial DC power supply system, REG systems and HVDC transmission system.

REFERENCES

- [1] E. Hossain, M. R. Tur, S. Padmanaban, S. Ay, and I. Khan, "Analysis and mitigation of power quality issues in distributed generation systems using custom power devices," *IEEE Access*, vol. 6, pp. 16816–16833, 2018.
- [2] B. B. Ambati and V. Khadkikar, "Optimal sizing of UPQC considering VA loading and maximum utilization of power-electronic converters," *IEEE Trans. Power Del.*, vol. 29, no. 3, pp. 1490–1498, Jun. 2014.
- [3] S. K. Khadem, M. Basu, and M. F. Conlon, "Intelligent islanding and seamless reconnection technique for microgrid with UPQC," *IEEE J. Emerg. Sel. Topics Power Electron.*, vol. 3, no. 2, pp. 483–492, Jun. 2015.
- [4] Y. Lu, G. Xiao, X. Wang, F. Blaabjerg, and D. Lu, "Control strategy for single-phase transformerless three-leg unified power quality conditioner based on space vector modulation," *IEEE Trans. Power Electron.*, vol. 31, no. 4, pp. 2840–2849, Apr. 2016.
- [5] S. Devassy and B. Singh, "Modified pq-theory-based control of solar-PV-integrated UPQC-S," *IEEE Trans. Ind. Appl.*, vol. 53, no. 5, pp. 5031–5040, Sep. 2017.
- [6] B. W. Franca, L. F. da Silva, M. A. Aredes, and M. Aredes, "An improved iUPQC controller to provide additional grid-voltage regulation as a STATCOM," *IEEE Trans. Ind. Electron.*, vol. 62, no. 3, pp. 1345–1352, Mar. 2015.
- [7] R. D. Middlebrook, "Null double injection and the extra element theorem," *IEEE Trans. Educ.*, vol. 32, no. 3, pp. 167–180, 1989.
- [8] V. Khadkikar, "Enhancing electric power quality using UPQC: A comprehensive overview," *IEEE Trans. Power Electron.*, vol. 27, no. 5, pp. 2284–2297, May 2012.
- [9] R. A. Modesto, S. A. O. da Silva, A. A. de Oliveira, and V. D. Bacon, "A versatile unified power quality conditioner applied to three-phase four-wire distribution systems using a dual control strategy," *IEEE Trans. Power Electron.*, vol. 31, no. 8, pp. 5503–5514, Aug. 2016.
- [10] R. J. M. dos Santos, J. C. da Cunha, and M. Mezaroba, "A simplified control technique for a dual unified power quality conditioner," *IEEE Trans. Ind. Electron.*, vol. 61, no. 11, pp. 5851–5860, Nov. 2014.
- [11] A. Mannan Rauf, A. Vilas Sant, V. Khadkikar, and H. H. Zeineldin, "A novel ten-switch topology for unified power quality conditioner," *IEEE Trans. Power Electron.*, vol. 31, no. 10, pp. 6937–6946, Oct. 2016.
- [12] S. B. Karanki, N. Gedddada, M. K. Mishra, and B. K. Kumar, "A modified three-phase four-wire UPQC topology with reduced DC-link voltage rating," *IEEE Trans. Ind. Electron.*, vol. 60, no. 9, pp. 3555–3566, Sep. 2013.
- [13] Q. Xu, F. Ma, A. Luo, Z. He, and H. Xiao, "Analysis and control of M3C-based UPQC for power quality improvement in medium/high-voltage power grid," *IEEE Trans. Power Electron.*, vol. 31, no. 12, pp. 8182–8194, Dec. 2016.
- [14] L. B. G. Campanhol, S. A. O. da Silva, A. A. de Oliveira, and V. D. Bacon, "Single-stage three-phase grid-tied PV system with universal filtering capability applied to DG systems and AC microgrids," *IEEE Trans. Power Electron.*, vol. 32, no. 12, pp. 9131–9142, Dec. 2017.
- [15] L. B. G. Campanhol, S. A. O. da Silva, A. A. de Oliveira, and V. D. Bacon, "Power flow and stability analyses of a multifunctional distributed generation system integrating a photovoltaic system with unified power quality conditioner," *IEEE Trans. Power Electron.*, vol. 34, no. 7, pp. 6241–6256, Jul. 2019.
- [16] Y. Li, Q. Liu, S. Hu, F. Liu, Y. Cao, L. Luo, and C. Rehtanz, "A virtual impedance comprehensive control strategy for the controllably inductive power filtering system," *IEEE Trans. Power Electron.*, vol. 32, no. 2, pp. 920–926, Feb. 2017.
- [17] Y. Li, Y. Peng, F. Liu, D. Sidorov, D. Panasetsky, C. Liang, L. Luo, and Y. Cao, "A controllably inductive filtering method with transformer-integrated linear reactor for power quality improvement of shipboard power system," *IEEE Trans. Power Del.*, vol. 32, no. 4, pp. 1817–1827, Aug. 2017.
- [18] J. Yu, Y. Li, Y. Cao, and Y. Xu, "An impedance-match design scheme for inductively active power filter in distribution networks," *Int. J. Elect. Power Energy Syst.*, vol. 99, pp. 638–649, Jul. 2018.
- [19] E. Jacobsen and R. Lyons, "The sliding DFT," *IEEE Signal Process. Mag.*, vol. 20, no. 2, pp. 74–80, Mar. 2003.
- [20] S. Golestan, M. Monfared, F. D. Freijedo, and J. M. Guerrero, "Performance improvement of a prefiltered Synchronous-Reference-Frame PLL by using a PID-type loop filter," *IEEE Trans. Ind. Electron.*, vol. 61, no. 7, pp. 3469–3479, Jul. 2014.
- [21] A. G. Yepes, F. D. Freijedo, J. Doval-Gandoy, Ó. López, J. Malvar, and P. Fernandez-Comesaña, "Effects of discretization methods on the performance of resonant controllers," *IEEE Trans. Power Electron.*, vol. 25, no. 7, pp. 1692–1712, Jul. 2010.
- [22] J. Zaragoza, J. Pou, S. Ceballos, E. Robles, C. Jaen, and M. Corbalan, "Voltage-balance compensator for a carrier-based modulation in the neutral-point-clamped converter," *IEEE Trans. Ind. Electron.*, vol. 56, no. 2, pp. 305–314, Feb. 2009.
- [23] S. K. Giri, S. Chakrabarti, S. Banerjee, and C. Chakraborty, "A carrier-based PWM scheme for neutral point voltage balancing in three-level inverter extending to full power factor range," *IEEE Trans. Ind. Electron.*, vol. 64, no. 3, pp. 1873–1883, Mar. 2017.
- [24] S. V. Kulkarni and S. A. Khaparde, *Transformer Engineering Design and Practice*. New York, NY, USA: Marcel Dekker, 2004, pp. 184–188.



JIAQI YU (Member, IEEE) was born in Liaoning, China, in 1989. She received the B.S. degree in electrical engineering from the North University of China, Taiyuan, China, in 2011, and the Ph.D. degree in electrical engineering from Hunan University, Changsha, China, in 2018.

Since 2019, she has been a Lecturer of electrical engineering with Changsha University. Her current research interests include power quality, renewable energy systems, and multilevel converters.



YONG XU was born in Inner Mongolia, China, in 1990. He received the B.S. degree in electrical engineering from the North University of China, Taiyuan, China, in 2011, and the Ph.D. degree in electrical engineering from Hunan University, Changsha, China, in 2017.

Since 2017, he was an Electrical Engineer with State Grid Hunan Integrated Energy Service Company Ltd., Changsha. His research interests include power quality, renewable energy systems, and integrated energy systems.



YONG LI (Senior Member, IEEE) was born in Henan, China, in 1982. He received the B.Sc. and Ph.D. degrees from the College of Electrical and Information Engineering, Hunan University, Changsha, China, in 2004 and 2011, respectively, and the Ph.D. degree from the Institute of Energy Systems, Energy Efficiency, and Energy Economics (ie3), TU Dortmund University, Dortmund, Germany, in June 2012.

In 2009, he has worked as a Research Associate with ie3, TU Dortmund University. He was a Research Fellow with The University of Queensland, Brisbane, QLD, Australia. Since 2014, he has been a Full Professor of electrical engineering with Hunan University. His current research interests include power system stability analysis and control, ac/dc energy conversion systems and equipment, analysis and control of power quality, and HVdc and FACTS technologies.



QIANYI LIU (Member, IEEE) was born in Sichuan, China, in 1992. He received the B.Sc. degree in electrical engineering and its automation (railway electrification) from Southwest Jiaotong University, Chengdu, China, in 2014, and the M.Eng. degree in electrical engineering from Hunan University, Changsha, China, in 2017, where he is currently pursuing the Ph.D. degree with the College of Electrical and Information Engineering. His research interests include electric

power optimization and control.

• • •